IEEE Access
Multidisciplinary | Rapid Review | Open Access Journal

Received April 11, 2020, accepted May 10, 2020, date of publication May 27, 2020, date of current version June 22, 2020.

Digital Object Identifier 10.1109/ACCESS.2020.2997968

A Novel Force-Controlled Spherical Polishing Tool Combined With Self-Rotation and Co-Rotation Motion

XIANG WU[1,2], ZHI HUANG[1], YONGJIAN WAN[2], HAITAO LIU[2], AND XIANG CHEN[1,2]
[1]School of Mechanical and Electrical Engineering, University of Electronic Science and Technology of China, Chengdu 611731, China
[2]Institute of Optics and Electronics, Chinese Academy of Sciences, Chengdu 610209, China

Corresponding author: Zhi Huang (zhihuang@uestc.edu.cn)

This work was supported by the National Key Research and Development Program of China under Grant 2016YFB0500400.

ABSTRACT In order to improve the polishing efficiency and aim at the problem that the positioning error of industrial robot will cause the fluctuation of polishing force and the instability of removal function, a novel force-controlled spherical polishing tool combined with self-rotation and co-rotation motion for automatic polishing process is presented. The spherical polishing tool, which is integrated into the end of arm of an industrial robot for workpiece profile polishing has a linear voice coil motor to provide compliance and polishing force in the polishing process. The fluctuation of the polishing force caused by the positioning error of the robot can be effectively reduced, and a stable symmetric Gaussian removal function can be obtained by optimizing the ratio of co-rotation to self-rotation speed of the end-effector. The main advantage of the polishing method is that the polishing force can be actively controlled according to the pre-planned polishing requirements. By measuring the responsiveness and the stability of the polishing force using the proposed end-effector, it is verified that the polishing method can better adapt to the fluctuation of the polishing force and has a good performance in achieving remarkable polishing force tracking. The effectiveness of the proposed polishing method in ensuring the stability of removal function and surface convergence efficiency is verified through polishing experiments. The robotic flexible polishing method has great application prospect in processing large-sized optical components. It significantly improves the precision of polishing force and the surface convergence efficiency of the workpiece.

INDEX TERMS Polishing force, robotic flexible polishing, removal function, spherical polishing tool.

I. INTRODUCTION

Polishing is frequently used as a precision machining process to improve the surface precision of workpieces. The polishing efficiency is a key factor, which directly affects the processing cycle and workpiece performance. However, the existing polishing processes, especially for complex curved components, mainly rely on manual polishing, which has the shortcoming of low processing efficiency, unstable polishing quality and poor working environment [1], [2]. In order to ensure the polishing efficiency and precision, computer controlled optical surfacing (CCOS) was proposed and this method makes the polishing process more precise and controllable [3].

Nowadays, many scholars have made fruitful achievements in the optical polishing based on the CCOS principle [4], [5]. Manual polishing is gradually replaced by computer numerically controlled (CNC) machines [6]. In addition, industrial robots have gradually played an important role in the polishing process. With remarkable positioning accuracy and force control performance, CNC machines are widely used for the polishing of various types of workpieces [7]. However, these machines frequently require special fixtures and techniques for the machining of complex shaped workpieces, and the limited available working space usually limits the size of the workpiece [8].

Huang *et al.* [9] reported that the application of industrial robots in automatic polishing process is one of the current development trends of flexible manufacturing technology. Industrial robots can not only integrate various types of end-effectors, but also have the advantages of low cost, large travel range and better posture control. Moreover, It can process different types of workpieces with large aperture and complex

The associate editor coordinating the review of this manuscript and approving it for publication was Shunfeng Cheng.

surfaces without using any special fixtures. Therefore, efficient and economical robotic polishing has attracted the attention of many researchers [10], [11]. The polishing force affects the quantitative processing of the workpiece, and it needs to be precisely controlled. Reference [12] also shows that although robotic polishing has the above advantages, the low joint stiffness and positioning accuracy are difficult to meet the accuracy requirements of precision machining equipment. It will cause the deviation between the actual polishing force and the theoretical value, and also affect the polishing precision and processing efficiency. Therefore, It has crucial practical significance to achieve the compliance between the robot polishing tool and workpiece in the polishing process.

Tian *et al.* [13] proposed an industrial robot polishing system. The polishing force of the system is detected and fed back through a force/torque sensor, and the polishing pressure is controlled by adjusting the robot's posture and position. Shi *et al.* [14] designed an automated polishing approach using a novel posture control mode to obtain a constant polishing pressure. Jin *et al.* [15] designed a gasbag polishing tool that is capable of adjusting air pressure and downward depth of the robot. These polishing methods implemented by the robot's controller have typical passive compliance, which can be represented as hybrid position/force control or impedance control method [16]. The precise force control and strict position control of the robot need to be implemented, and the existence of the force-position coupling makes the control of the robot more complicated and difficult. In addition, the robot itself cannot respond to the force fluctuations, and the strong specificity of passive compliant devices limits its application [17]. Due to the shortcomings of passive control, active compliance control is required.

Some researchers have proposed that the active compliance control approach can be used [18]. Reference [19] revealed that the polishing force adjustments of the around-the-arm's force control system are performed by the polishing tool. This polishing method has lower inertia, faster response and higher bandwidth of the system compared with the through-the-arm technique. Liao *et al.* [20] proposed a polishing tool whose force is adjusted by three pneumatic cylinders, which are evenly distributed on the polishing tool. Cheng *et al.* [21] designed a machine-type magnetorheological polishing tool, and its main characteristic is a dual-axis wheel which is driven by a gearbox. The rotation of the wheel around the horizontal axis and the revolution around vertical axis are respectively driven by different motors. The polishing tool has a large inertia and does not have force control performance, and it is not suitable as a robot polishing tool.

Yu and Fang [22] controlled the cating force between the lapping tool and workpiece through using the binocular visual serving and force feedback. The polishing force of the polishing tools proposed in reference [23] and reference [24] is controlled by a combination of linear motor and force sensor. Wang and Lin [25] designed a miniaturized polishing tool, and the polishing force is controlled by a belt drive system.

To achieve remarkable polishing force tracking, we designed a novel force-controlled spherical polishing tool combined with self-rotation and co-rotation motion, and the polishing force is directly controlled by the end-effector. The effectiveness of the polishing tool is demonstrated by the experimental results. In this paper, we first established the mathematical theoretical modeling and introduced the design of the proposed polishing tool in Section 2. The system modeling and polishing force characteristics are described in Section 3. The stability of material removal function and actual polishing results for the proposed polishing method are depicted in Section 4. Finally, the conclusion and the possible future work are given at the end.

II. THEORETICAL MODELING AND STRUCTURAL DESIGN OF THE PROPOSED POLISHING TOOL

A. THEORETICAL MODELING

The material removal at any point on the workpiece is determined by material removal function and dwell time of the polishing tool along the polishing path on the workpiece surface. The material removal on the workpiece can be expressed by the well known relationship called the Preston's equation [26]:

$$R(x, y) = \frac{1}{T} K \int_0^T P(x, y) \cdot V(x, y) \cdot dt. \tag{1}$$

where $R(x, y)$ is the material removal function which is defined as the material removal generated by polishing tool in unit time;T is polishing time;K is the Preston coefficient, which is related to the processing conditions such as the material characteristics of the workpiece and polishing tool, polishing liquid and environment;$V(x, y)$ and $P(x, y)$ are the relative polishing speed and polishing pressure between the polishing tool and the workpiece respectively. To obtain the removal function modeling, we established the instantaneous geometric motion relationship of the contact area between the workpiece and the proposed polishing tool.

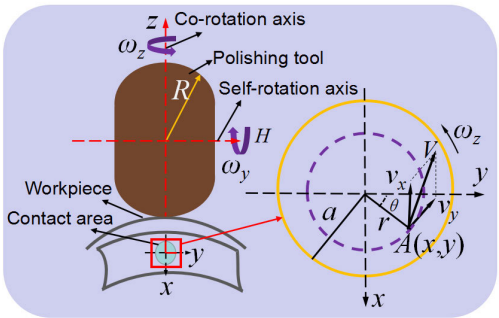

FIGURE 1. Schematic diagram of the spherical polishing tool.

As shown in Fig. 1, ω_z is the angular velocity of the co-rotation motion (around the Z-axis). ω_y is the angular velocity of the self-rotation motion (around the H-axis). v_x is the velocity vector generated by self-rotation motion and v_y is

the co-rotation velocity vector at arbitrary point $A(x, y)$ of the polishing head.

The spherical polishing tool can be regarded as an elastic body and the workpiece surface is assumed to be rigid and flat. Since the shape of the polishing head is spherical, its two principle radii of curvature are equal. According to the Hertz spherical contact theory [27], the circular radius of the contact area is related to the polishing force, the radius of the polishing head, and the material characteristics of the part and polishing head. The corrected instantaneous pressure distribution obeys the following equation [10]:

$$P(x, y) = \frac{5F}{2\pi a^2}\left[1 - \left(\frac{x^2}{a^2} + \frac{y^2}{a^2}\right)\right]^{\frac{3}{2}}. \tag{2}$$

The radius (a) of the tool-workpiece contact area can be defined as equation (3), and F is the polishing force which is applied to the workpiece by the proposed end-effector.

$$a = \left(\frac{3(d_1 + d_2)RF}{4}\right)^{\frac{1}{3}}. \tag{3}$$

where R is the radius of the proposed spherical polishing tool. d_1 and d_2 can be calculated by (4).

$$d_i = \frac{1 - \mu_i^2}{E_i^2}, \quad i = 1, 2. \tag{4}$$

where E_1, E_2 and μ_1, μ_2 are the elastic modulus and Poisson's ratio of the spherical tool head and the workpiece respectively. Since the contact area is small, it is assumed that the velocity vectors generated by self-rotation motion in the contact area can be regarded as identical. The velocity vector of point $A(x, y)$ can be represented as

$$V(x, y) = v_x + v_y. \tag{5}$$

In equation (5)

$$v_x = \omega_y \times R. \tag{6}$$

$$v_y = \omega_z \times r. \tag{7}$$

where r is the polar radius of the arbitrary point $A(x, y)$ in the contact area. Substituting equations (6)∼(7) into equation (5), the polishing absolute velocity is

$$V(x, y) = \sqrt{\left(|\omega_y| R\right)^2 + (|\omega_z| r)^2 + 2|\omega_y| R |\omega_z| r \cos\theta}. \tag{8}$$

where θ is the angle between v_x and v_y. It can be easily known from the geometric relationship of triangles that the angle in equation (8) is equal to the θ angle shown in Fig. 1. In addition, θ is the product of ω_z and polishing time, that is, $\theta = |\omega_z| \cdot T$. Substituting equation (2) and equation (8) into equation (1), the removal function can be defined as

$$R(r) = \frac{5FK}{2\Omega\pi a^2} \int_0^{\Omega} \left(1 - \frac{r^2}{a^2}\right)^{3/2} \cdot \sqrt{\left(|\omega_y| R\right)^2 + (|\omega_z| r)^2 + 2|\omega_y| R |\omega_z| r \cos\theta} \cdot d\theta. \tag{9}$$

here, $\Omega = T |\omega_z|$.

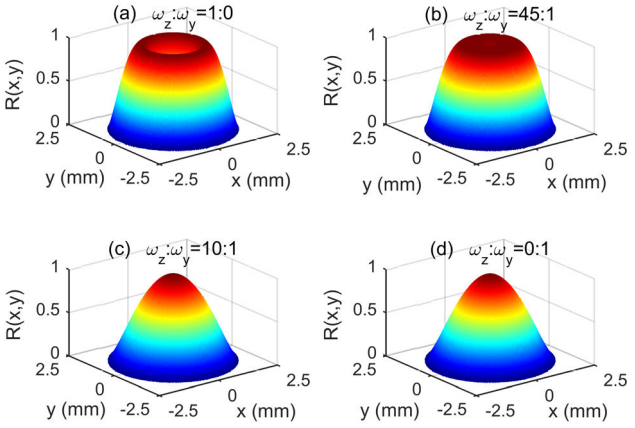

FIGURE 2. The removal functions for different velocity ratos.

The shapes of the normalzed removal functions for different angular velocity ratios ($\omega_z : \omega_y$) are shown in Fig. 2. When the velocity ratio is relatively large, the profile of the removal function is concave. As the ratio decreases, the removal function tends to be a symmetric Gaussian shape. Moreover, when the ratio is less than 10, the shapes of the removal functions are similar, and it indicates that the removal function is more stable under this conditions. At the same time, the existence of the self-rotation motion can prevent the velocity and material removal at the center of the contact area from being zero.

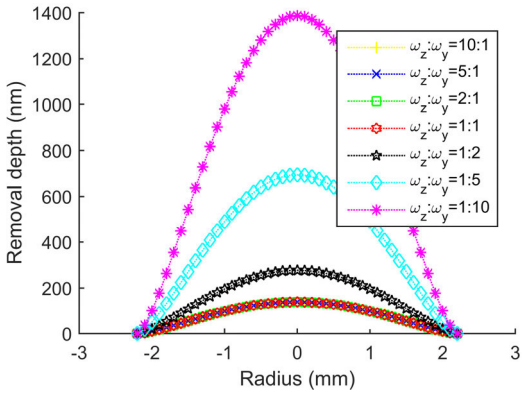

FIGURE 3. 2D profiles of the removal functions.

According to the Preston hypothesis, the material removal can be calculated as the convolution between the dwell time and removal function, which preferably presents a symmetrical Gaussian shape. Reference [28] indicated that a stable symmetrical removal function not only contributes to planing the polishing path, but also helps to optimize the dwell-time distribution. As shown in Fig. 3, when the ratio is in the range of 1 to 10, the profiles of the removal functions are substantially coincident, and it indicates that the material removal efficiency has been less affected by the co-rotation motion. Furthermore, when the ratio is less than 1, with the co-rotation velocity increasing, the polishing efficiency increases gradually. Therefore, in order to obtain a symmetrical Gaussian

removal function and have a high material removal efficiency, the angular velocity ratio (ω_z : ω_y) of the polishing tool designed in this paper was selected as 1: 4.

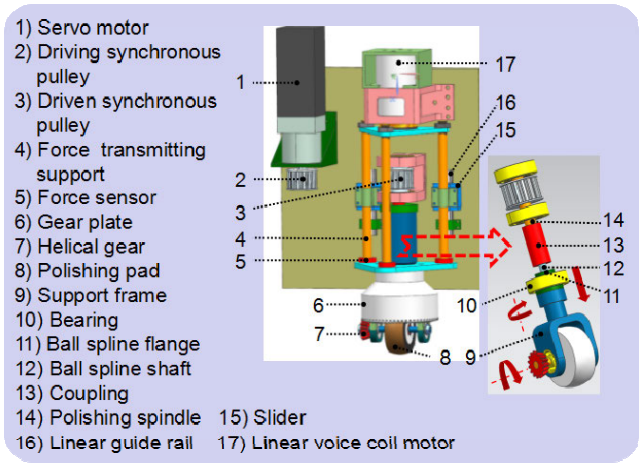

FIGURE 4. The mechanical structure of the force-controlled spherical polishing tool.

B. STRUCTURAL DESIGN

Figure 4 shows the three-dimensional assembly drawing of the mechanical structure of the proposed force-controlled spherical polishing tool combined with self-rotation and co-rotation motion. It is mainly composed of a rotating mechanism and an electric control mechanism. The polishing tool is mounted to the end of an industrial robot as an end-effector and its position is controlled by the robot. The end-effector is responsible for controlling the axial force to achieve the polishing of the workpiece. As shown in Fig 4, The driven synchronous pulley is connected to the driving synchronous pulley through a synchronous belt. The polishing spindle mounted to the driven synchronous pulley is connected to the ball spline shaft through a coupling. The ball spline flange is fixed to the support frame through bolts. The synchronous pulley is driven by the servo motor to rotate, and the support frame with a polishing head makes a co-rotation motion. At the same time, the helical gear rolls on a fixed gear plate and the polishing tool obtains a self-rotation motion. The polishing force between the polishing pad and the workpiece is controlled by a linear voice coil motor. The polishing force is stably transmitted to the polishing area through three force transmitting supports. During the polishing process, the polishing force is measured by the force sensors. The force transmitting supports connected to a slider can move on a linear guide rail in the direction of force. The existence of the ball spline, sliders and linear guide rails enables the end-effector to obtain the decoupling between the co-rotation motion of the polishing tool and the vertical motion controlled by the force. The outer layer of the spherical polishing head is a polyurethane polishing pad. This method improves the tool compliance and reduces the impact of low stiffness and low positioning resolution of industrial robot on the polishing force.

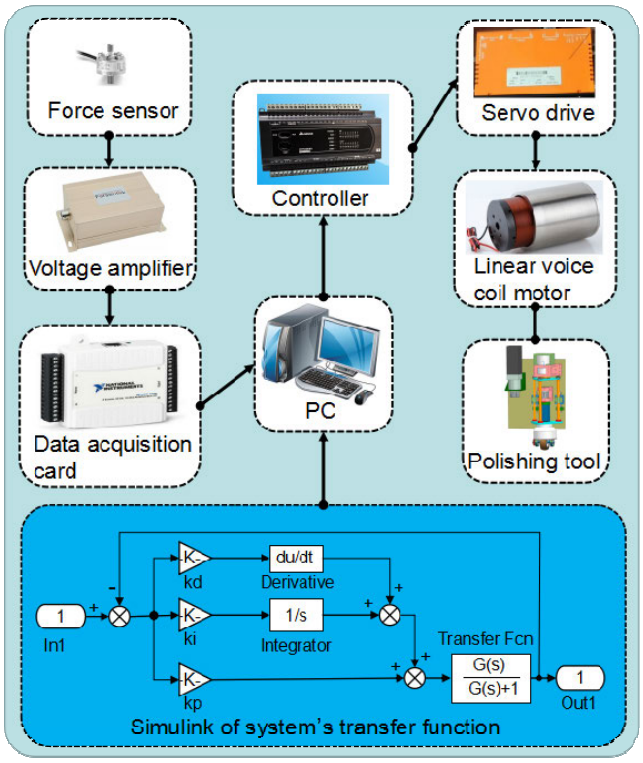

FIGURE 5. The control system hardware (upper part) and software (lower part) used to implement the force control of the designed polishing tool.

III. SYSTEM MODELING AND POLISHING FORCE CHARACTERISTICS

A. SYSTEM MODELING

The designed polishing tool is mounted to the end of an industrial robot, which performs machining operations based on predetermined polishing trajectories. Fig. 5 (upper part) shows schematically the control system hardware, which is used to control the polishing force of the proposed polishing tool. During the polishing process, the polishing force between the polishing tool and workpiece is measured by the force sensor. The force signal amplified by the amplifier is collected by the data acquisition card. The polishing force between the end-effector and the workpiece can be controlled by the system in real time. In this study, for the linear voice coil motor with a current control mode, the control voltage signal is proportional to the motor current. The relationship between the force provided by the motor and the control voltage signal within the specified working range of the motor is as follows:

$$f_m = K_m u. \tag{10}$$

where f_m, K_m and u are the force generated by the linear voice coil motor, force sensitivity of the motor and control voltage signal, respectively. Considering the inertia load f_G of the polishing tool, the actual polishing force f measured by the force sensor can be expressed as

$$f = f_m + f_G. \tag{11}$$

The needed polishing force is given as f_n, and the force tracking error e_f of the polishing tool is

$$e_f = f_n - f. \tag{12}$$

Substituting Eqs. (10) and (11) into (12), the polishing force tracking error e_f can be expressed as follows:

$$e_f = f_n - K_m u - f_G. \tag{13}$$

In order to reduce the polishing force tracking error from the modeling error, the controller is proposed as

$$u = \left(f_n - f_G + K_p e_f + K_i \int_0^t e_f dt + K_d \frac{de_f}{dt}\right) \Big/ K_m. \tag{14}$$

where K_p, K_i and K_d are the proportional, integral and derivative gains, respectively.

In this paper, the linear voice motor (model No. VCAR0140-0150-00A) is selected with a stroke of 15 mm and a force constant coefficient of 26.7 N/A. The model is mass-damped type with a differential equation of the system shown below:

$$m\ddot{x} = f_m + f_G - f_d - f_c. \tag{15}$$

where f_d is dynamic friction and f_c is damping force of the polishing tool. In the actual polishing process, the sliding friction is negligible and the gravity can be balanced by the supporting force. The system has the following relationship:

$$\begin{cases} m\ddot{x} = K_m i_a - c\dot{x} \\ u = L_a \dfrac{d_{i_a}}{d_t} + R_a i_a + K_m \ddot{x}. \end{cases} \tag{16}$$

where m, x, i_a, L_a, R_a and c are the mass of mover and its connected parts, displacement of mover, current of motor, inductance of motor, resistance of motor and damping coefficient of the system, respectively.

By performing Laplace Transform on the differential equations of the system, the open-loop transfer function of the system can be obtained:

$$G(s) = \frac{x(s)}{u(s)} = \frac{K_m}{L_a m s^3 + (R_a m + L_a c)s^2 + (R_a c + K_m^2)s}. \tag{17}$$

Neglecting the inductance parameter of the electromechanical system, the closed-loop transfer function of the system can be expressed as

$$\phi(s) = \frac{G(s)}{G(s) + 1}. \tag{18}$$

The analysis model shown in the lower part of Fig. 5 can be established in simulink. By analyzing the dynamic model of the robotic force-control polishing tool designed in this paper, the frequency domain characteristics of the closed-loop system are shown in Fig 6. As shown in Fig. 6, the frequency response of the polishing tool is attenuated to 0 dB with a frequency of 900 rad/s. Therefore, the bandwidth frequency of the polishing tool's actuator is relatively high.

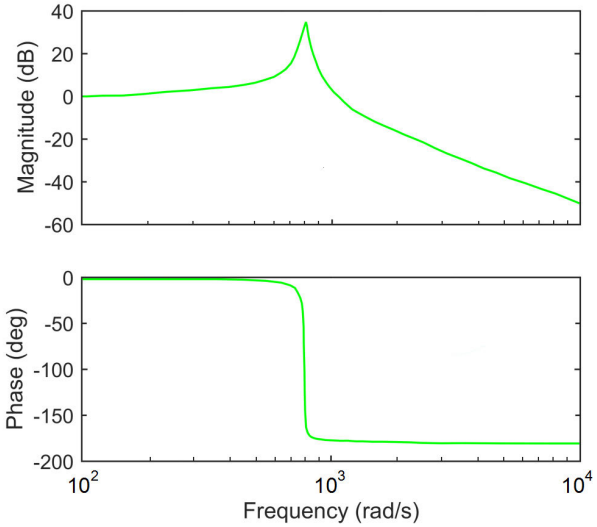

FIGURE 6. Frequency characteristic Bode diagram.

B. THE STEP RESPONSE CHARACTERISTIC

It can be seen from the measured robot position error that in order to achieve precise control of the polishing force and reduce the force error caused by the position fluctuation, it is necessary to have a high force response in time of polishing the workpiece. The proposed end-effect is attached to the robotic arm (Fig. 7). The polishing force is detected through a force detecting platform (accuracy 1%) [30]. The step response curves of the polishing force in the range of 10∼40 N are shown in Fig. 8.

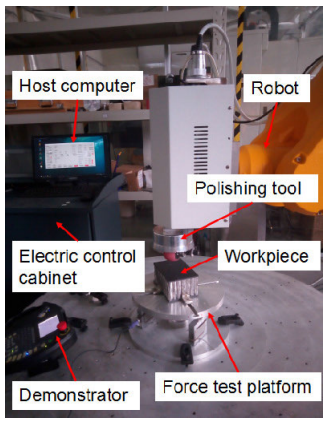

FIGURE 7. The detection of the polishing force.

According to Fig. 8, the proposed polishing tool has a step response time about 0.1 s with the force in the range of 10∼40 N, and its response speed is as high as 200 N/s. For another, the response curves of the polishing force adjusted by using the positioning of robotic joints are shown in Fig. 9 [13]. Although the polishing forces are small (2 N and 3 N), the polishing method (through-the-arm force control) has longer settling time and bigger overshoot of the polishing force. The fast response for this polishing method using the proposed polishing tool improves the processing efficiency. Furthermore, small overshoot can effectively reduce

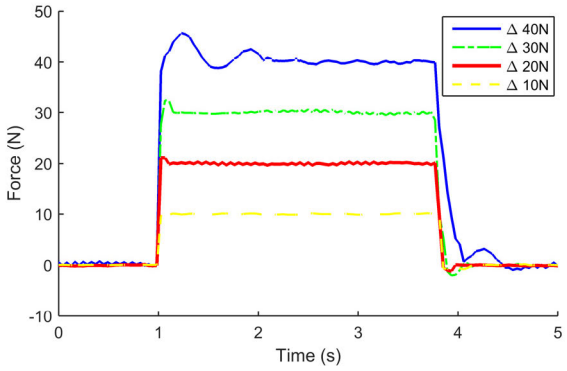

FIGURE 8. The step response curves of the polishing force.

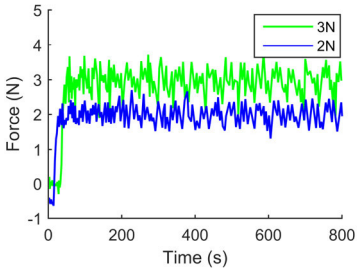

FIGURE 9. The real-time polishing force during polishing processing.

workpiece damage. This also proves that it can better achieve the response of the polishing force to the position error of industrial robot in the polishing process. Besides, as shown in Fig. 8, when the force value is greater than 30 N, the response speed becomes slower with the increasing of the polishing force. Therefore, in order to ensure a high force response and improve the stability of removal function, the polishing force should be controlled to be less than 30 N.

C. THE STABILITY CHARACTERISTIC OF POLISHING FORCE

In the actual processing process, the polishing force is one of the important process parameters. Apart from the response speed of polishing force, its accuracy and stability can directly affect the roughness of the polished workpiece. Figure 10 shows the fluctuation curves of the polishing force in different conditions (the fixed point polishing/Static and the polishing using a spiral path/Dynamic). The force value is in the range of 10∼60 N.

As shown in Fig. 10, the actual polishing force fluctuation is close to the theoretical value, and the error amplitude increases with the increase of the force. In addition, compared with the static state, the force error and changing frequency in the dynamic state are larger. This situation may be due to the effects of the uneven surface of the workpiece. When the force is in the range of 10 N to 40 N, the relative error of the polishing force is less than 5%. Moreover, the force fluctuation range of the proposed end-effector is less than 10%, and the experiment results show that the polishing force has great stability.

To verify the effectiveness of the proposed polishing method, we compared it with the polishing force response

TABLE 1. Experimental conditions.

ω_z	ω_y	Polishing force	Dwell time	Slurry
90 rpm	360 rpm	5 N	10 s	Al_2O_3 aqueous solution

proposed by Liu [31]. When the polishing force (25 N) is adjusted by the pneumatic cylinder, the response curves of fixed point polishing and spiral polishing are shown in Fig. 11. The magnitude of the polishing force is large, especially when a spiral polishing path is used. Due to the interference of the cylinder piston on the system, the polishing force has a lower valley value. It is not conducive to the deterministic polishing of the workpiece and also shows that this polishing method using the proposed polishing tool in this paper has certain advantages.

IV. POLISHING EXPERIMENT RESULTS AND DISCUSSION

A. THE STABILITY OF MATERIAL REMOVAL FUNCTION

According to the Preston theory and the constructed material removal modeling as described above, the polishing force error will directly affect the polishing process. The fluctuation of the removal function will cause a difference between the theoretical removal and the actual removal of the workpiece. Therefore, the stability of the removal function determines whether the surface accuracy of the workpiece converges or not. In order to verify the effectiveness of the proposed end-effector on polishing force control, five sets of fixed spot polishing experiments were conducted on a SiC specimen with a diameter of 130 mm. Meanwhile, the stability of the removal function was analyzed. The experimental conditions are listed in Table 1. As shown in Fig. 12, the actual material removal profile of the polishing spot is a symmetric Gaussian shape, which is consistent with the simulation results.

The five sets of removal functions were divided by their respective peak value to get the normalized removal functions. The normalized actual removal functions and the theoretical profile are shown in Fig. 13. The theoretical removal function is more plump, and it may be due to the fact that the rotation motion of the proposed polishing tool makes it difficult for some slurry to immerse into the polished area. In addition, the wear of the polishing pad leads to the change of the contact state between the polishing head and the workpiece during the actual polishing process. The volume removal rates of the fixed point polishing experiments vary from 80.22 to 80.45 μm $\cdot$ mm^2/min, and its error fluctuation is only 0.27%. The experimental results indicate that the removal function using this polishing method is stable and its effectiveness in polishing force control is verified.

B. POLISHING PROCESS

To explore the actual performance of the proposed robotic polishing method using the spherical polishing tool combined with self-rotation and co-rotation motion, a parabolic carbon-fiber workpiece was polished. The effective aperture

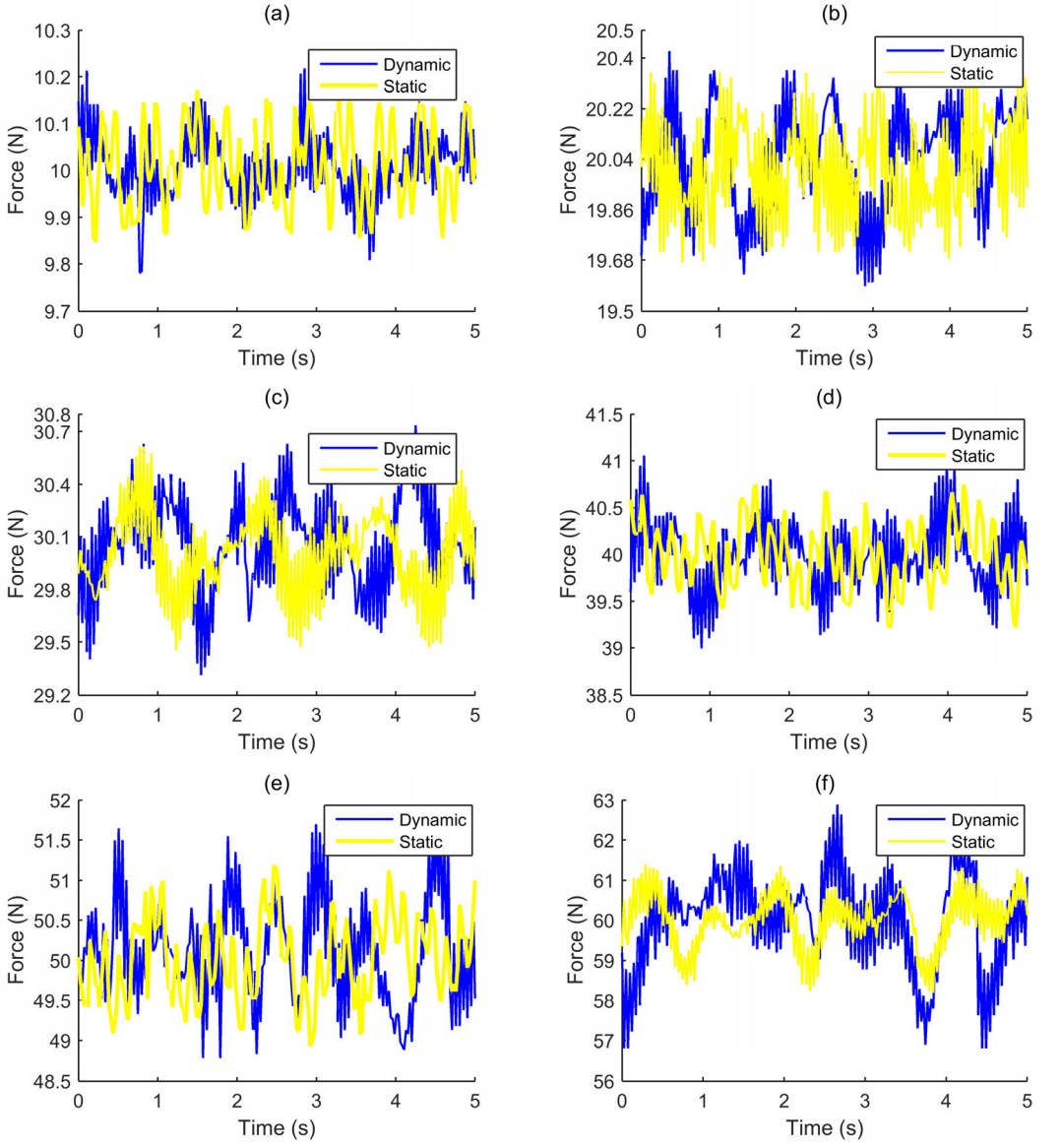

FIGURE 10. The step response curves of the polishing force: (a) 10N; (b) 20N; (c) 30N; (d) 40N; (e) 50N; (f) 60N.

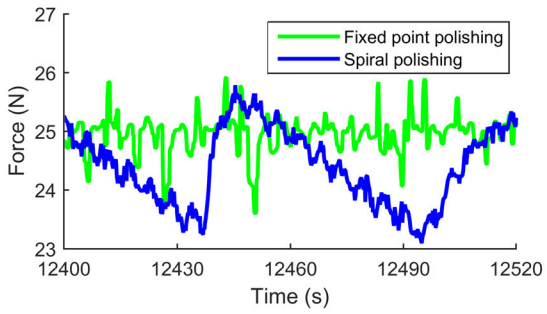

FIGURE 11. Pneumatic response of fixed point polishing and spiral polishing.

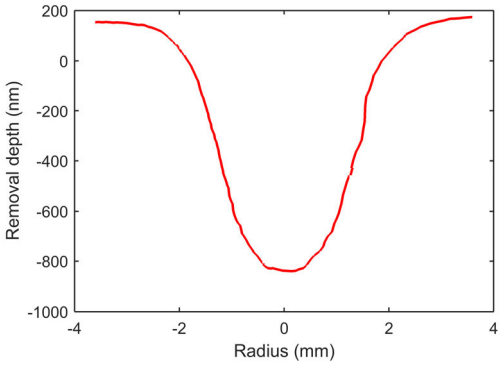

FIGURE 12. The actual material removal profile.

of the workpiece is 5 m, the focal length is 2000 mm and the central aperture is 300 mm. For the purpose of improving polishing efficiency, the rough polishing was first conducted. The self-rotation speed is 600 rpm, the co-rotation speed is 150 rpm, the polishing force is 15 N and the robot feed

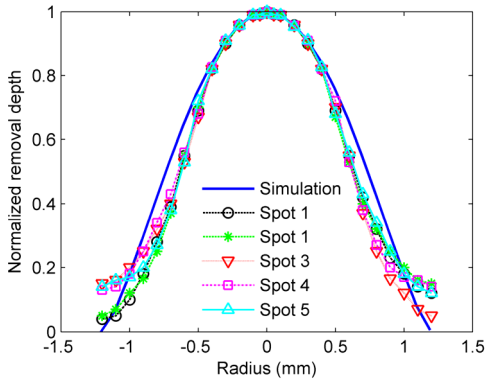

FIGURE 13. The normalized actual removal functions and the theoretical profile.

speed is 2 mm/s. The workpiece surface is measured by a coordinate measuring machine. After 10 cycles of rough polishing, the surface accuracy of the workpiece is improved from 277.680 μm PV (29.943 μm RMS) to 22.136 μm PV (3.032 μm RMS), and the convergence rate of the rough polishing process is fast.

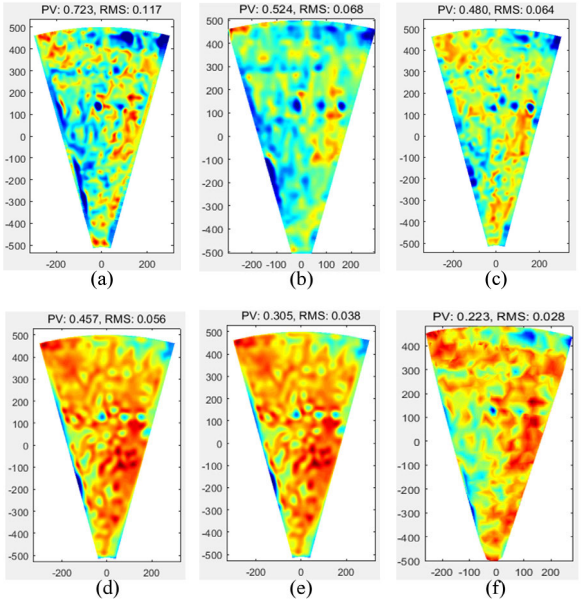

FIGURE 14. The convergence process of the workpiece surface: (a) initial surface; (b) after 2nd cycle; (c) after 4th cycle; (d) after 6th cycle; (e) after 8th cycle; (f) after 10th cycle.

In order to improve the surface precision, the rough-polished workpiece is smoothed and the precision polishing experiment is conducted. The self-rotation speed is 360 rpm, the co-rotation speed is 90 rpm, the polishing force is 5 N and the feed speed of the robot is 1 mm/s. The convergence process of the precision polishing is shown in Fig. 14. As demonstrated in Fig. 14, after 10 cycles of precision polishing, the form error is improved from 0.723 μm PV (0.117 μm RMS) to 0.223 μm PV (0.028 μm RMS), and the higher surface accuracy is achieved.

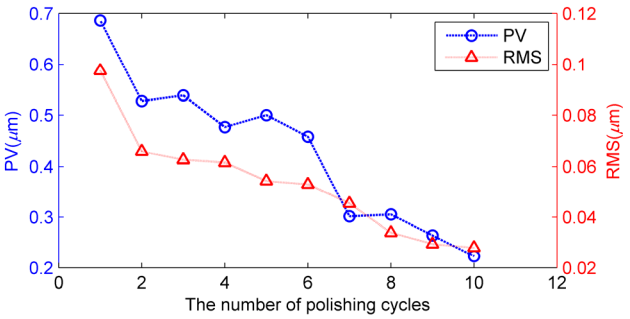

FIGURE 15. The convergence curves of the workpiece surface: (a) PV value; (b) RMS value.

Fig. 15 shows the convergence curves of the precision polishing. In the early stage of the processing cycles, the PV and RMS values are decreased rapidly, the surface accuracy of the carbon-fiber workpiece is greatly improved and the remarkable polishing efficiency can be obtained. In the middle of the processing cycles, the PV and RMS values are gradually reduced overall and the convergence rate of the surface accuracy decreases. Finally, the directional texture of the workpiece surface is removed, and a high surface accuracy can be obtained. The effectiveness of the proposed robotic polishing method using the spherical polishing tool combined with self-rotation and co-rotation motion is verified.

V. CONCLUSION AND FUTURE WORKS

Various automatic polishing technologies play an important role in the modern precision industries. Robotic polishing has broad application prospects due to its unique advantages. During the polishing process, the polishing force is a key factor affecting the surface roughness. The positioning error of the robot will change the required contact condition between the end-effector and workpiece, and it thereby affect the actual polishing force. In this paper, a novel force-controlled spherical polishing tool combined with self-rotation and co-rotation motion is presented.

The polishing force is controlled by the contraction and extension of the voice coil motor on the end-effector, and this polishing method has a higher compliance for the robotic polishing tool. The effectiveness of the proposed robotic polishing method was verified by the experiments. It can be seen from the fixed point polishing experiments that the symmetrical Gaussian removal function can be obtained by optimizing the angular velocity ratio of the polishing head, and the removal function is relatively stable. We detected the ability of the proposed end-effector to track the polishing force, and the force fluctuation curves were obtained. The experimental results show that this polishing method has large response speed and smaller force overshoot. The remarkable convergence ability of the proposed robotic polishing tool is verified by the polishing experiments.

The advantage of the proposed polishing method is that the end-effector can be integrated into the robotic arm to directly control the force, and it can reduce the influence of the positioning error of industrial robot on the polishing force.

Both the research on the suppression of the mid-frequency errors using a designed Gaussian-perturbed polishing path and the process optimization using the robotic polishing tool proposed in this paper will be presented in a separate. In future work, in order to achieve non-constant polishing force process, reduce the time of polishing cycle and improve polishing efficiency, the instantaneous polishing force will be adjusted in real time on the basis of the form error. In addition, because there are some screwing and rotation actions during the robot manipulation process, a predictive approach for sensorless bimanual teleoperation under random time delays with adaptive fuzzy control will also be studied.

REFERENCES

[1] L. Liang and F. Xi, "A linearized model for control of automated polishing process," in *Proc. IEEE Conf. Control Appl.*, Aug. 2005, pp. 28–31.

[2] F. Tian, C. Lv, Z. Li, and G. Liu, "Modeling and control of robotic automatic polishing for curved surfaces," *CIRP J. Manuf. Sci. Technol.*, vol. 14, pp. 55–64, Aug. 2016.

[3] R. A. Jones, "Optimization of computer controlled polishing," *Appl. Opt.*, vol. 16, no. 1, pp. 218–224, Jan. 1997.

[4] F.-J. Shiou and A. Asmare, "Parameters optimization on surface roughness improvement of zerodur optical glass using an innovative rotary abrasive fluid multi-jet polishing process," *Precis. Eng.*, vol. 42, pp. 93–100, Oct. 2015.

[5] T. Arnold and F. Pietag, "Ion beam figuring machine for ultra-precision silicon spheres correction," *Precis. Eng.*, vol. 41, pp. 119–125, Jul. 2015.

[6] E. Pitschke, M. Schinhaerl, R. Rascher, P. Sperber, L. Smith, R. Stamp, and M. Smith, "Simulation of a complex optical polishing process using a neural network," *Robot. Comput.-Integr. Manuf.*, vol. 24, no. 1, pp. 32–37, Feb. 2008.

[7] Y. Kakinuma, K. Igarashi, S. Katsura, and T. Aoyama, "Development of 5-axis polishing machine capable of simultaneous trajectory, posture, and force control," *CIRP Ann.*, vol. 62, no. 1, pp. 379–382, 2013.

[8] A. E. K. Mohammad and D. Wang, "Electrochemical mechanical polishing technology: Recent developments and future research and industrial needs," *Int. J. Adv. Manuf. Technol.*, vol. 86, nos. 5–8, pp. 1909–1924, Sep. 2016.

[9] H. Huang, L. Zhou, X. Q. Chen, and Z. M. Gong, "SMART robotic system for 3D profile turbine vane airfoil repair," *Int. J. Adv. Manuf. Technol.*, vol. 21, no. 4, pp. 275–283, Feb. 2003.

[10] S. Ji, G. Zheng, M. Jin, L. Zhang, W. Zhang, and H. Hou, "Study on measuring method and distribution law of stress of contact area between bonnet polishing tool and workpiece," *Mech. Eng. China.*, vol. 22, no. 9, pp. 1107–1111, Jan. 2011.

[11] A. El Khalick Mohammad and D. Wang, "A novel mechatronics design of an electrochemical mechanical end-effector for robotic-based surface polishing," in *Proc. IEEE/SICE Int. Symp. Syst. Integr. (SII)*, Dec. 2015, pp. 127–133.

[12] D. D. Walker, D. Brooks, A. King, R. Freeman, R. Morton, G. McCavana, and S.-W. Kim, "The 'Precessions' tooling for polishing and figuring flat, spherical and aspheric surfaces," *Opt. Express*, vol. 11, no. 8, pp. 958–964, May 2003.

[13] F. Tian, Z. Li, C. Lv, and G. Liu, "Polishing pressure investigations of robot automatic polishing on curved surfaces," *Int. J. Adv. Manuf. Technol.*, vol. 87, nos. 1–4, pp. 639–646, Oct. 2016.

[14] Y. Shi, D. Zheng, L. Hu, Y. Wang, and L. Wang, "NC polishing of aspheric surfaces under control of constant pressure using a magnetorheological torque servo," *Int. J. Adv. Manuf. Technol.*, vol. 58, nos. 9–12, pp. 1061–1073, Feb. 2012.

[15] M. Jin, S. Ji, Y. Pan, H. Ao, and S. Han, "Effect of downward depth and inflation pressure on contact force of gasbag polishing," *Precis. Eng.*, vol. 47, pp. 81–89, Jan. 2017.

[16] M. H. Raibert and J. J. Craig, "Hybrid position/force control of manipulators," *J. Dyn. Syst. Meas. Control.*, vol. 102, no. 2, pp. 126–133, 1980.

[17] P. Kryczka, K. Hashimoto, A. Takanishi, and P. Kormushevet, "Walking despite the passive compliance: Techniques for using conventional pattern generators to control instrinsically compliant humanoid robots," in *Proc. Int. Conf. CLAWAR*, Aug. 2013, pp. 487–494.

[18] D. Zheng, B. D. Lv, J. M. Zhan, and L. Y. Hu, "Study on force control in abrasive polishing of aspheric parts," *Appl. Mech. Mater.*, vols. 37–38, pp. 1287–1291, Nov. 2010.

[19] G. M. Bone and M. A. Elbestawi, "Active end effector control of a low precision robot in deburring," *Robot. Comput.-Integr. Manuf.*, vol. 8, no. 2, pp. 87–96, Jan. 1991.

[20] L. Liao, F. Xi, and K. Liu, "Modeling and control of automated polishing/deburring process using a dual-purpose compliant toolhead," *Int. J. Mach. Tools Manuf.*, vol. 48, nos. 12–13, pp. 1454–1463, Oct. 2008.

[21] H. Cheng, Y. Feng, T. Wang, and Z. Dong, "Magnetorheological finishing of optical surface combined with symmetrical tool function," *Frontiers Optoelectron. China*, vol. 3, no. 4, pp. 408–412, Nov. 2010.

[22] M. Yu and S. Fang, "The dynamics of the system for the constant force polishing on the double-robot," in *Proc. IEEE Int. Conf. Technol. Mech. Eng.*, Oct. 2017, pp. 110–114.

[23] A. E. K. Mohammad, J. Hong, and D. Wang, "Design of a force-controlled end-effector with low-inertia effect for robotic polishing using macro-mini robot approach," *Robot. Comput.-Integr. Manuf.*, vol. 49, pp. 54–65, Feb. 2018.

[24] U. Satake, T. Enomoto, Y. Obayashi, and T. Sugihara, "Reducing edge roll-off during polishing of substrates," *Precis. Eng.*, vol. 51, pp. 97–102, Jan. 2018.

[25] H. Wang and W. Lin, "Removal model of rotation & revolution type polishing method," *Precis. Eng.*, vol. 50, pp. 515–521, Oct. 2017.

[26] F. W. Preston, "The theory and design of plate glass polishing machines," *J. Glass Technol.*, vol. 11, no. 44, pp. 214–256, 1927.

[27] L. Zong, B. Xie, and A. Wang, "Modeling and simulation of wheeled polishing method for aspheric surface," *Proc. SPIE*, vol. 9683, Oct. 2016, Art. no. 968313.

[28] M. Schinhaerl, R. Rascher, R. Stamp, G. Smith, L. Smith, E. Pitschke, and P. Sperber, "Filter algorithm for influence functions in the computer controlled polishing of high-quality optical lenses," *Int. J. Mach. Tools Manuf.*, vol. 47, no. 1, pp. 107–111, Jan. 2007.

[29] H. Han, Z. Zeng, H. Liu, and H. Zhao, "Measurement and analyses on positioning accuracy for optical processing robots," *Opto-Electron. Eng.*, vol. 44, no. 5, pp. 516–522, 2017.

[30] Z. Huang, S. Chen, and H. Wang, "Development of three-dimensional dynamic grinding force measurement platform," *Proc. Inst. Mech. Eng., C, J. Mech. Eng. Sci.*, vol. 232, no. 2, pp. 331–340, Nov. 2016.

[31] F. Liu, "Design of pressure control system for the head of large scale optical polishing robot," M.S. thesis, Dept. Automat., Chongqing Univ., Chongqing, China, 2015.

XIANG WU received the B.E. degree from the Mechanical Engineering Institute, Chongqing University of Technology, in 2017. He is currently pursuing the master's degree with the School of Mechanical and Electrical Engineering, University of Electronic Science and Technology of China. His research interests include mechanism design, control, and robotic machining.

ZHI HUANG received the B.E., M.S., and Ph.D. degrees from the Department of Mechanical and Electronic Engineering, Chongqing University, in 2000, 2005, and 2010, respectively. He is currently an Associate Professor with the School of Mechanical and Electrical Engineering, University of Electronic Science and Technology of China. His research interests include advanced manufacturing equipment, robotic polishing, and high-precision measurement technique.

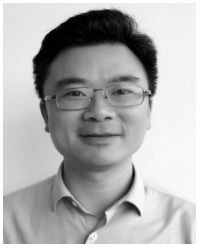

YONGJIAN WAN received the B.E. degree from the Mechanical Engineering Institute, Chongqing University, in 2000, and the Ph.D. degrees from the Institute of Optics and Electronics, Chinese Academy of Sciences, in 2007. He is currently the Director of the Advanced Optics Development Center, Institute of Optics and Electronics, Chinese Academy of Sciences. His research interests include advanced optical manufacturing and optical measurement technique.

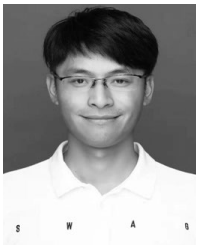

HAITAO LIU received the B.E. degree from the School of Information and Communication Engineering, Zhongbei University, in 2009, and the Ph.D. degree from the Institute of Optics and Electronics, Chinese Academy of Sciences, in 2014. His research interests include robotics, mechatronics, and optical manufacturing.

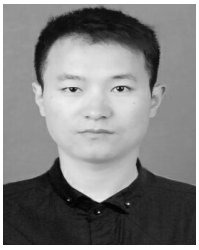

XIANG CHEN received the B.E. degree from the Mechanical Engineering Institute, Qingdao University of Technology, in 2015, and the M.S. degree from the School of Mechanical and Electrical Engineering, University of Electronic Science and Technology of China, in 2018. His research interests include mechanism design, optical processing equipment, and robotic manipulation.